

HOSTED BY



ELSEVIER

Contents lists available at ScienceDirect

Progress in Natural Science: Materials International

journal homepage: www.elsevier.com/locate/pnsmi

Original Research

High efficiency synthesis of HKUST-1 under mild conditions with high BET surface area and CO₂ uptake capacity

Yipei Chen^{a,b}, Xueliang Mu^{a,c}, Edward Lester^b, Tao Wu^{a,c,*}^a New Materials Institute, The University of Nottingham Ningbo China, Ningbo 315100, China^b Department of Chemical and Environmental Engineering, The University of Nottingham, Nottingham NG7 2RD, UK^c Municipal Key Laboratory of Clean Energy Conversion Technologies, The University of Nottingham Ningbo China, Ningbo 315100, China

ARTICLE INFO

Keywords:

Metal organic framework
HKUST-1
Rapid synthesis
Green synthesis
CO₂ adsorption

ABSTRACT

This study focuses on the development of a hydrothermal method for the rapid synthesis of good quality copper benzene-1,3,5-tricarboxylate (referred to as HKUST-1) with high yield under mild preparation conditions to address the issues associated with reported methods. Different synthesis conditions and activation methods were studied to understand their influence on the properties of HKUST-1. It was found that mixing the precursors at 50 °C for 3 h followed by activation via methanol refluxing led to the formation of a product with the highest BET specific surface area of 1615 m²/g and a high yield of 84.1%. The XRD and SEM data illustrated that the product was highly crystalline. The sample was also tested on its capacity in CO₂ adsorption. The results showed strong correlation between surface area of the sample and its CO₂ uptake at 1 bar and 27 °C. The HKUST-1 prepared in this study demonstrated a high CO₂ uptake capacity of 4.2 mmol/g. It is therefore concluded that this novel and efficient method can be used in the rapid preparation of HKUST-1 with high surface area and CO₂ uptake capacity.

1. Introduction

Metal Organic Frameworks (MOFs) are hybrid materials that consist of organic ligands and metal ions or metal-contained clusters [1,2]. Compared with traditional porous solid adsorbents (such as zeolites, activated carbon and N-doped porous carbons [3]), MOFs possess the highest surface area among many porous materials known to date [4]. Furthermore, the structure and pore size of MOF materials are relatively easier to tune for specific applications [5]. In recent years, MOFs have been found to show great potential in CO₂ capture [6,7]. HKUST-1 (Cu₃(BTC)₂) is one of the most widely studied MOFs owing to its high surface area and large pore volume [8], which was firstly reported by Chui [9] in 1999. This Cu-based material consists of copper nodes and organic ligands (benzene-1,3,5-tricarboxylate, BTC), with each copper coordinated with four oxygen atoms and water molecules [9]. This framework contains a bimodal pore size distribution, i.e. a large cage with 9 Å diameter and small pores with 3.5 Å diameter [10,11].

In the past few years, various synthesis strategies were reported, such as microwave-assisted synthesis [12,13], ultrasonic synthesis [11,14], mechanochemical synthesis [15] and conventional hydro/solvothermal synthesis. Conventional methods normally involve the use

of high temperature and pressure [16] to facilitate the formation of MOFs in shorter period of time [17] or require a long reaction time (from days to weeks [5,18]) to achieve the synthesis of MOFs under milder conditions. The other methods rely on the use of specific instruments, such as high pressure autoclave, which is usually associated with safety issues and high costs. The surface area reported in literature ranges from 400 to 1800 m²/g, while most are within the range of 700–1000 m²/g [19–22]. Al-Janabi et al. reported an optimised procedure for the synthesis of HKUST-1, which led to the production of HKUST-1 with a yield of 89.4% and Brunauer-Emmett-Teller (BET) surface area of 1507 m²/g. However, the MOF was prepared in a sealed autoclave at 100 °C which meant that elevated pressure was unavoidable, and the preparation process required 24 h to complete. More recently, McKinstry et al. [23] also adopted hydrothermal methods to produce HKUST-1 with a high surface area, but the yield was rather low especially when only ethanol was used as the solvent and only achieved 55% when DMF was used as the solvent. In summary, most recent methods involve the adoption of elevated pressure and result in the formation of products with either low yields or low surface areas. Table 1 summarizes the operating conditions and properties of HKUST-1 synthesized using different hydrothermal methods.

Peer review under responsibility of Chinese Materials Research Society.

* Corresponding author.

E-mail address: Tao.Wu@nottingham.edu.cn (T. Wu).<https://doi.org/10.1016/j.pnsc.2018.08.002>

Received 19 March 2018; Received in revised form 13 August 2018; Accepted 13 August 2018

Available online 01 September 2018

1002-0071/ © 2018 Chinese Materials Research Society. Published by Elsevier B.V. This is an open access article under the CC BY-NC-ND license (<http://creativecommons.org/licenses/by-nc-nd/4.0/>).

Table 1
Comparison of HKUST-1 synthesized using different hydrothermal methods.

Years	Pressure	Time (h)	Temperature (°C)	Solvents	Yield (%)	S_{Langmuir} (m ² /g)	S_{BET} (m ² /g)
1999 [9]	Elevated pressure in an autoclave	12	180	EtOH/H ₂ O	60.0	918	692
2012 [19]	Elevated pressure in an autoclave	18	110	EtOH/H ₂ O	N/A	N/A	1055
2015 [24]	Atmospheric pressure	12	80	DMF	92.0	N/A	1387
2015 [25]	Elevated pressure in an autoclave	24	120	EtOH/H ₂ O	N/A	N/A	1140
2015 [26]	Elevated pressure in an autoclave	24	100	EtOH	89.4	N/A	1507
2017 [23]	Low pressure	5	60	EtOH	41.6	2100	N/A
2017 [23]	Low pressure	5	79	DMF	55.0	1200	N/A

To date, very few HKUST-1 synthesis methods have been reported to operate under atmospheric pressure. In the past few years, Khoshhal et al. [24] produced HKUST-1 under atmospheric pressure with dimethyl formamide (DMF) as the solvent. However, these methods resulted in either a low yield or surface area. Therefore, there is still a need to develop new methods for the preparation of MOFs with high surface area and high yield under mild preparation conditions, which can also have high CO₂ uptake capacity.

In this study, a high efficiency solvothermal method was developed for the synthesis of HKUST-1 under atmospheric pressure and low temperature. The characterization of MOFs was conducted to optimize conditions for the synthesis of HKUST-1 with a high yield and high BET surface area. The HKUST-1 was also tested in terms of its potential in CO₂ adsorption.

2. Experimental

2.1. Materials and preparation method

All chemicals used in this study were purchased from Sigma Aldrich and used without further purification. In a typical synthesis process, copper nitrate trihydrate (98%) and benzene-1,3,5-tricarboxylic acid (95%) were mixed and heated to 50 °C for 3 h. Upon cooling to room temperature, it was placed in a dryer operated at 120 °C for 12 h. The dried powder was then activated by using either methanol or ethanol to wash out the impurities trapped in pores. Finally, the product was centrifuged and dried at 120 °C. Table 2 lists the denominations of different products prepared in this study.

2.2. Characterization

Powder X-ray diffraction (XRD) patterns were recorded using a Bruker D8 A25 diffractometer operated at 40 kV and 35 mA between 5°2 θ and 40°2 θ with a Cu K α radiation. The scanning speed was 1 s/step and the step size was 0.02° [27]. Thermal stability test was performed using a thermogravimetric analyser (NETZSCH STA49 F3) following the procedure described by Zhang et al. [28]. Approximately 10 mg sample was heated from 30 to 900 °C at a heating rate of 10 K/min under high-purity nitrogen (99.999%) atmosphere. The morphology of materials was observed using a scanning electron microscope (SEM, ZEISS Sigma VP) operated at 20 kV [29,30]. Nitrogen adsorption experiment was performed using a Micromeritics Tristar 3020 instrument operated at 77k [31]. Before each test, the sample was degassed at 150 °C for 12 h.

Table 2
List of HKUST-1 samples and corresponding preparation conditions.

Sample ID	Reaction condition	Activation condition	Drying condition
T1-N	3 h, 50 °C	No activation	12 h, 120 °C
T1-E1	3 h, 50 °C	3 h	12 h, 120 °C
T2-E1	9 h, 50 °C	3 h, ethanol	12 h, 120 °C
T1-E1-2	3 h, 50 °C	3 h, ethanol	12 h, 120 °C
T1-M1	3 h, 50 °C	3 h, methanol	12 h, 120 °C
T1-M2	3 h, 50 °C	3 h, methanol twice	12 h, 120 °C

2.3. CO₂ adsorption-desorption test

The CO₂ uptake capacity was examined at 1 bar using the TGA (NETZSCH STA49 F3). As with a typical test, the temperature was initially raised to 150 °C under N₂ atmosphere (99.999%) and kept isothermal for 30 min, followed by cooling to 27 °C and kept isothermal for another 30 min. After the temperature became stable, the gas flow was switched to pure CO₂ for 30 min. The CO₂ cyclic adsorption-desorption test was performed to evaluate the stability of HKUST-1. In this cyclic test, N₂ gas was used to purge off the adsorbed CO₂ in sample at the same temperature. The adsorption and desorption processes were repeated for 10 times continuously. The N₂ gas flow rate was set at 100 mL/min and CO₂ at 133 mL/min. Blank group was conducted for every test to eliminate the influence of buoyancy. Moreover, CO₂ isothermal adsorption test was carried out using a Micromeritics ASAP 2020 instrument at 27 °C for 12 h, followed the procedure described elsewhere [32].

3. Results & discussion

3.1. Characterization of crystal structure

It can be seen from Fig. 1 that the main X-ray diffraction peaks for each sample matched well with the patterns obtained from the simulation based on single crystal data, as well as those reported in the literature [33]. The sharp peaks for all samples suggested that the sample possessed high degree of crystallinity [33].

The color of as-synthesized HKUST-1 powder was light blue, but turned into dark blue after activation by ethanol or methanol. The color change in sample is consistent with those reported in literature [26]. According to Cheng et al. [34], this change implies that the co-ordination number of copper has decreased from six to four. The activation process eluted the coordinated solvent or water from the copper sites.

There is a small difference observed from the comparison with simulated patterns. The intensity ratios of (331) to (420) plane, and (200) to (220) plane are both notably higher for the simulated patterns, which can be as attributed to dehydrated samples. This phenomenon is in agreement with that reported by Schlichte et al. [16]. It is very difficult to avoid this difference because HKUST-1 rapidly adsorbs moisture from the air during the preparation process of the XRD test. Kathuria et al. [35] stated that the marked reduction of peak intensities of (111) and (200) is related to the FCC crystal structure loss on account of HKUST-1 hydration.

From the SEM images (as shown in Fig. 1), no significant morphological differences were observed among these activated samples. The crystal sizes are all in the range of 100–500 nm. The SEM image of T1-M2 clearly shows crystal surface defects and smaller particle size when compared with T1-M1, suggesting the second washing process has significant influence on the structure of the HKUST-1 and damages the surface. These damages also affect surface area and CO₂ capacity of the sample.

The XRD pattern of the sample without activation (T1-N) was significantly different from the activated samples. T1-M1 was taken as the benchmark to compare with T1-N. As shown in Fig. 2, there are three

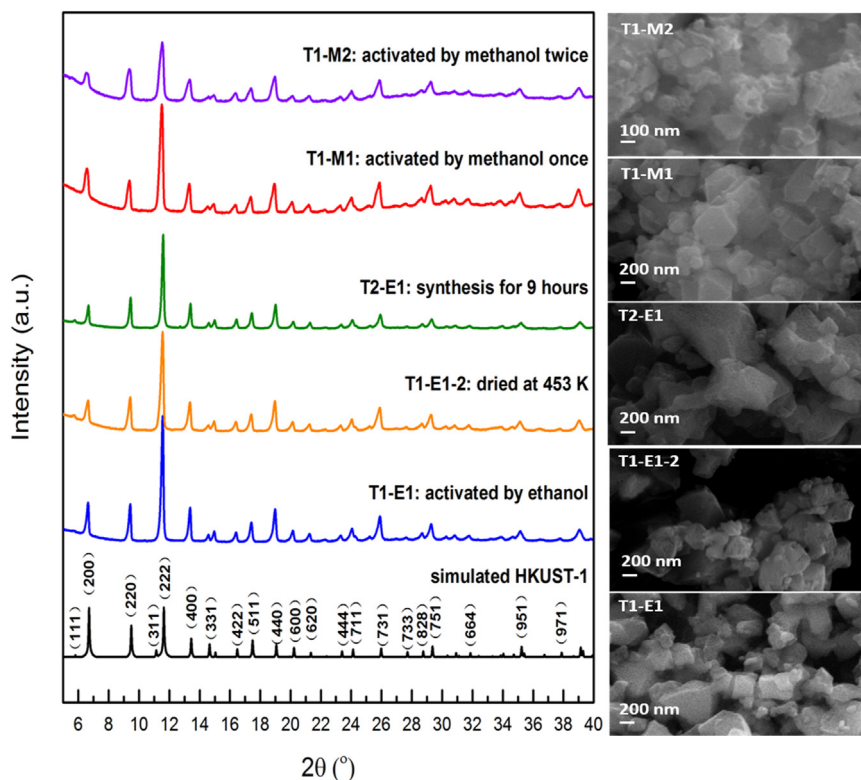


Fig. 1. XRD patterns and SEM images of the samples synthesized under different reaction conditions.

main distinctive peaks at $2\theta = 7.9^\circ, 10.7^\circ, 12.7^\circ$. The unreacted copper nitrate and trimesic acid may have remained in the samples. In addition, the diffraction data of simulated $\text{Cu}_2(\text{OH})_3\text{NO}_3$ indicated their presence in the sample. It is also reported [36] that the copper based precursors include $\text{Cu}_2(\text{OH})_3\text{NO}_3$, which might be trapped in the HKUST-1 sample. However, after taking these impurities into consideration, the pattern of T1-N was still not consistent with that of HKUST-1. This result suggested that new crystalline complex were formed via chemical bindings [37]. The activation process has broken these bonding and therefore the XRD showed the pure phase HKUST-1. Moreover, the pH value of T1-M1 solution was measured as 0.68, and 7.22 for T1-M2 solution. These solutions were collected from the upper layer after centrifugation of each sample. The significant difference in pH value indicated that the first-time activation removed impurities trapped in the sample.

3.2. Thermogravimetric analysis

Fig. 3 presents the weight loss of samples being heated from room temperature to 600°C at a heating rate of 10°C per minute in nitrogen atmosphere. The shapes of their respective TGA curves are similar to those reported for HKUST-1 crystals [5,38].

In the TGA profile, the first mass loss stage that occurred between 30 and 110°C can be ascribed to the evaporation of physically adsorbed water. When exposed to air, HKUST-1 can instantaneously adsorb water into the pores and occupy the 96 j position [9,16]. This amount of water can be driven off when the sample is heated to 110°C .

The two samples activated by ethanol (T1-E1, T2-E1) showed an obvious weight loss in stage (II) between 110 and 250°C , which indicates the release of water that is chemically bonded on copper atoms, and solvent that is physically adsorbed in internal pores [16]. This is

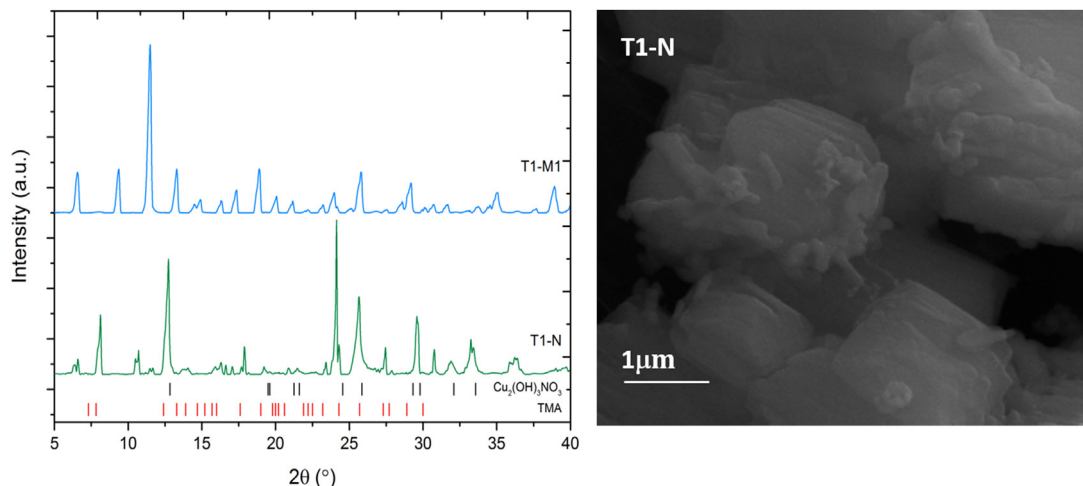


Fig. 2. Comparison of the non-activated sample and the sample activated once using methanol.

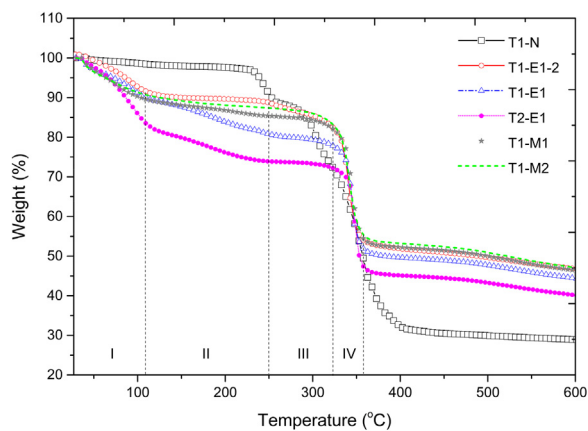


Fig. 3. Thermogravimetric analysis of various samples.

consistent with that reported by Lestari et al. [20]. The coordination bonds between water and copper require a higher temperature (150–300 °C) to break, which is higher than the temperature needed for physically adsorbed water molecules to be released upon heating.

It is obvious that the samples activated by methanol showed a small weight loss in this stage, whereas the sample without activation (T1-N) exhibited a plateau in the temperature range from 30 to 230 °C. This indicates that no solvent was physically adsorbed in the pores. This can be explained by the non-porous structure of T1-N, which was examined by the N_2 adsorption experiment discussed in the next part. Hence, it is possible that the guest molecules released in stage II are formed during the ethanol activation process. It should be noted that the sample activated by using ethanol which underwent drying at 180 °C (T1-E1-2) exhibited no obvious mass loss upon heating. This suggests that the higher drying temperature could eliminate guest molecules, but on the other hand, it might also lead to the formation of more defects on the framework.

All activated samples only showed a small weight loss in stage III and started to breakdown when temperature was raised further to above 320 °C (stage IV), which is attributed to the damage of the relatively weak coordination bond between copper and the ligands [39,40]. However, for the sample without washing and activation, the weight loss occurred in a broader region as a result of the residuals, such as unreacted chemicals mixed in the product, that were trapped in pores. Powder XRD analysis showed the compositions of the decomposed sample after being heated to 600 °C, which were Cu, Cu_2O and CuO . This is consistent with those reported in literature [16]. It can therefore be concluded that methanol is a better activation agent than ethanol since the sample activated by methanol contained much lesser impurities than those washed by ethanol. Methanol can be exchanged with guest molecules trapped inside the pore system at a higher efficiency than ethanol.

3.3. Textual properties

N_2 adsorption-desorption isotherms at 77 K are shown in Fig. 4. The non-activated sample exhibited a plateau with almost zero N_2 adsorption, indicating its non-porous structure. Isotherm curves with similar shapes were found for the samples such as T1-M1, T2-E1, T1-E1 and T1-E1-2. The adsorption equilibria were quickly reached in the low relative pressure region, and there were no hysteresis loops shown under high relative pressure. This shape indicates that it is Type I isotherm according to the IUPAC (International Centre for Theoretical and Applied Chemistry) classification [22,41]. Normally, samples with Type I isotherm are of microporous (< 2 nm) structure [15].

BET surface area and porosity properties of samples are listed in Table 3. The sample activated once by methanol showed the highest BET surface area of 1616 m^2/g . Its total pore volume and micropore

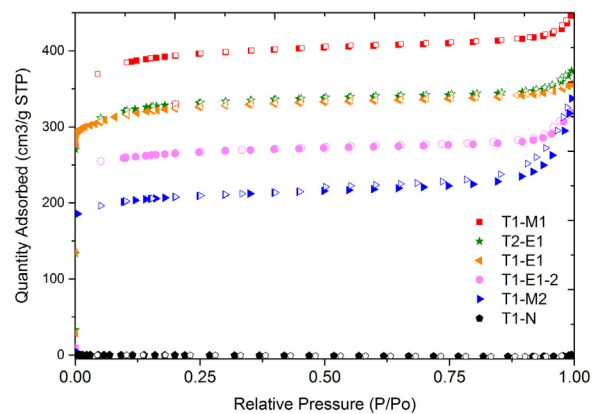


Fig. 4. N_2 adsorption-desorption isotherms for different samples.

Table 3

Textural properties of different HKUST-1s.^a

Sample ID	S_{BET} (m^2/g)	$S_{Langmuir}$ (m^2/g)	V_p (cm^3/g)	V_m (cm^3/g)
T1-N	0	0	–	–
T1-E1	1268	1475	0.55	0.51
T1-E1-2	1052	1208	0.49	0.41
T2-E1	1274	1501	0.58	0.51
T1-M1	1615	1806	0.69	0.61
T1-M2	801	972	0.52	0.31

^a V_p : total pore volume at 0.99 p/p_0 , V_m : micropore volume by t-plot analysis.

volume were determined to be 0.69 and 0.61 cm^3/g , respectively. These values are relatively high as compared with the reported results (as shown in Table 1). The high gas uptake capacity suggested that the guest molecules in the pores were removed after activation process [42], which is also consistent with the TGA results. The surface areas of T1-E1 and T2-E1 were very similar, so were the pore volumes. Therefore, it is suggested that mixing time does not have significant influence on the textural properties of sample and thus three-hour mixing is adequate. However, T1-E1-2 is of a much lower surface area, which is attributed to the drying process. The BET surface area of T1-M2 is about half that of the T1-M1. It can be seen from Fig. 4, T1-M2 presented a hysteresis loop in the high relative pressure region, which was attributed to the stacking of particles or capillary condensation occurring in the mesopores (2–50 nm) [43,44]. The mesopores were formed in the second washing process while the micropore structure was ruined to some extent. The BET and porosity results suggested that methanol is a better activation agent than ethanol for purifying the sample. This can be attributed to the smaller size of methanol molecules thus making it easier to exchange with the molecules trapped in the pores. In addition, optimisation involves washing once with methanol to achieve a high surface area and to avoid damages to the micropores.

3.4. CO_2 adsorption and structure stability

More often than not, the high surface area of MOFs is a significant feature which leads to a high CO_2 uptake capacity [4]. In addition, HKUST-1 contains unsaturated metal sites (also known as open metal sites) with relatively strong affinity towards CO_2 [45,46]. Therefore, this study aims to examine the CO_2 adsorption performance of HKUST-1 prepared in this study and any enhancement resulted from this novel approach.

The CO_2 adsorption was carried out using a TGA under atmospheric pressure. Different temperatures were tested to investigate the influence of temperature on CO_2 uptake. Fig. 5 shows the amount of CO_2 adsorbed on the T1-M1 at 27, 50, 70, 90 and 110 °C. It was found that CO_2 uptake was 8.08%, which is relatively high as compared with data

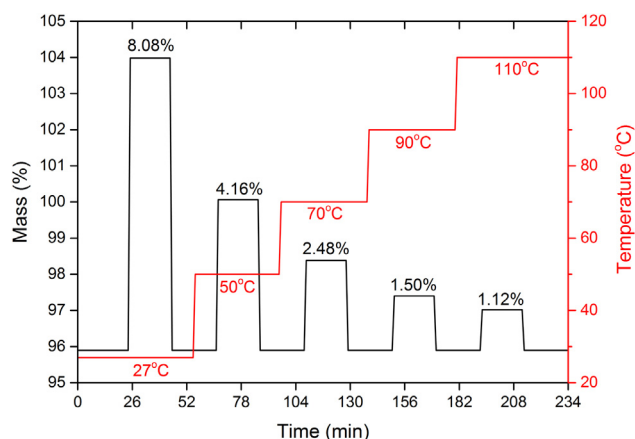


Fig. 5. CO₂ uptake at different temperatures.

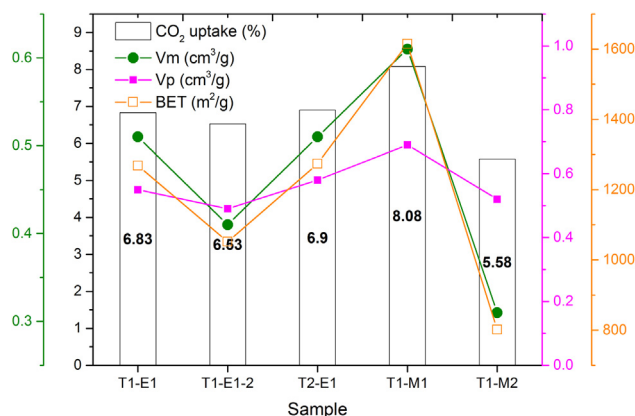


Fig. 6. Relationship between CO₂ capacity and total pore volume, micropore volume and BET surface area.

reported by others [41,47]. Fig. 6 illustrates the relationship between the textural properties of MOFs and CO₂ uptake. It is clear that textural property has strong influence on CO₂ uptake. T1-M1, which possesses the highest CO₂ uptake capacity (8.08% or 1.84 mmol/g) among the five samples, has the highest V_m, V_p as well as BET surface area.

The CO₂ adsorption isotherm curve of the sample with the highest surface area (T1-M1) is shown in Fig. 7. The test was conducted at 27 °C and low pressure in order to match the post-combustion CO₂ capture application environment, since the partial pressure of CO₂ in the flue gas is often around 1 bar or lower [46,48]. The result shows that under

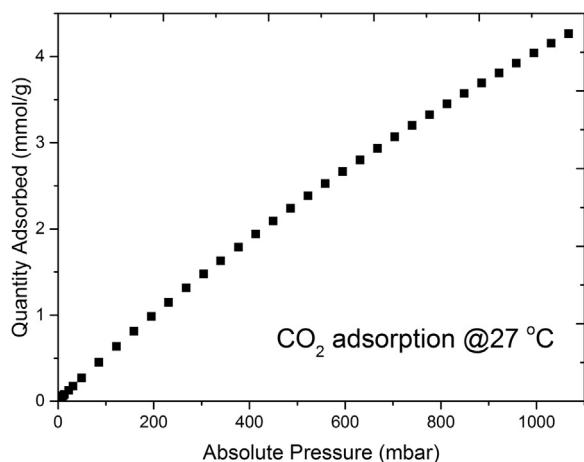


Fig. 7. CO₂ isotherm curve at ambient temperature.

Table 4
CO₂ adsorption capacity of various MOFs.

MOF name	Adsorption capacity (mmol/g)	Adsorption condition	Reference
HKUST-1	1.82	30 °C, 10 bar	
HKUST-1	3.27	25 °C, 103 kPa	[49]
HKUST-1	4.20	27 °C, 1 bar	This study
HKUST-1	4.50	22 °C, 0.9 bar	[50]
MIL-101(Cr)	1.17	30 °C, 10 bar	[41]
ZIF-8	0.76	25 °C, 1 bar	[52]
UIO-66(Zr)	2.70	25 °C, 2 bar	[53]
NUT-6	3.70	25 °C, 1 bar	[54]

1 bar the HKUST-1 synthesized in this study was able to adsorb 4.2 mmol/g (equals to 18.5%) of CO₂. This value is much higher than that obtained in this study using TGA (8.08% or 1.84 mmol/g). This is believed to be due to the sample being degassed in advance before CO₂ adsorption isotherm was obtained, thus releasing more sites for CO₂ uptake.

It was reported [49] that at atmospheric temperature and pressure, CO₂ uptake capacity of some commonly used MOFs varies from 2.9 to 5.1 mmol/g. Table 4 shows the comparison of HKUST-1 synthesized in this study with reported data in terms of CO₂ adsorption performance. Compared with most previously reported HKUST-1 samples, the product synthesized in this work showed a relatively higher CO₂ adsorption capacity. Although the absolute amount of CO₂ uptake was slightly lower than the HKUST-1 reported by Wang et al. [50], the reported adsorption temperature was 22 °C, which was 5 °C lower than the adsorption temperature adopted in this study (27 °C). This could be a reason for the slightly higher performance recorded by Wang et al. since CO₂ uptake ability is highly favored by lower temperatures [51].

In addition, compared with the other widely studied adsorbents listed in Table 4, the HKUST-1 prepared in this study showed superior adsorption capability under similar adsorption conditions. This is ascribed to its unsaturated metal centers with stronger physisorption affinity towards CO₂. Therefore, it can be concluded that HKUST-1 prepared in this study is promising in the CO₂ adsorption [46,48].

Since the structural stability of the adsorbent is another significant factor to be considered in CO₂ adsorption applications, the CO₂ cyclic adsorption-desorption test of T1-M1 was conducted and the results are shown in Fig. 8. The amount of CO₂ adsorbed by the MOF of each cycle was almost the same, suggesting that with N₂ feeding CO₂ was almost completely outgassed and the product can be regenerated for further adsorption of CO₂. Moreover, the product retained its structural integrity after multiple cycles. This finding suggests that the HKUST-1 synthesized in this study could be regenerated without losing its CO₂ uptake capacity. The reversible adsorption also demonstrates that the

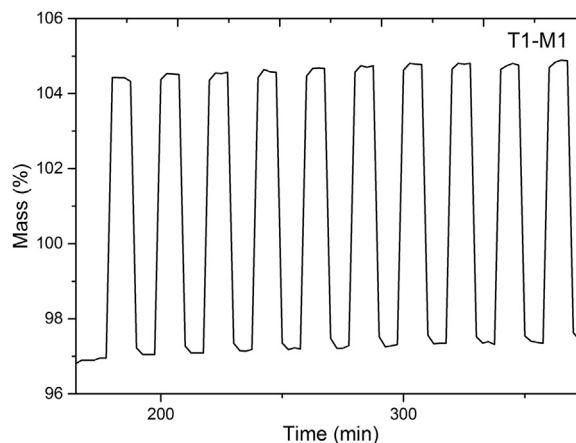


Fig. 8. CO₂ cyclic adsorption for the optimal sample T1-M1.

interaction between metal and CO₂ does not involve chemical bonding [45]. This stability agrees well with other researchers' cyclic tests on MOFs [55,56].

4. Conclusion

In this study, a new method has been developed for the rapid and highly efficient synthesis of HKUST-1 MOFs with high surface area (1615 m²/g). This method allows the synthesis of HKUST-1 to be carried out safely under ambient pressure and mild temperature leading to a high yield of MOFs at 84.1%. In addition, the CO₂ adsorption tests showed that the HKUST-1 prepared in this study has a good CO₂ uptake capacity of 4.2 mmol CO₂/g.

Acknowledgements

The Ministry of Science and Technology, China is acknowledged for partially sponsoring this research under its National Key R&D Programme (2017YFB0603202). The University of Nottingham UK and the University of Nottingham Ningbo China are acknowledged for providing the first two authors with full scholarships.

References

- [1] Z.-G. Gu, J. Zhang, Epitaxial growth and applications of oriented metal-organic framework thin films, *Coord. Chem. Rev.* (2017).
- [2] Z.G. Gu, D.J. Li, C. Zheng, Y. Kang, C. Wöll, J. Zhang, *Angew. Chem. Int. Ed.* 56 (24) (2017) 6853–6858.
- [3] J. Kou, L.-B. Sun, *Ind. Eng. Chem. Res.* 55 (41) (2016) 10916–10925.
- [4] Y. Liu, Z.U. Wang, H.-C. Zhou, *Greenh. Gases: Sci. Technol.* 2 (4) (2012) 239–259.
- [5] L.H. Wee, M.R. Lohe, N. Janssens, S. Kaskel, J.A. Martens, *J. Mater. Chem.* 22 (27) (2012) 13742–13746.
- [6] J.L.C. Rowsell, O.M. Yaghi, *Microporous Mesoporous Mater.* 73 (1–2) (2004) 3–14.
- [7] Y. Jin, C. Zhao, Y. Lin, D. Wang, L. Chen, C. Shen, *J. Mater. Sci. Technol.* 33 (8) (2017) 768–774.
- [8] D. Zhang, Y. Xu, Q. Liu, Z. Xia, *Inorg. Chem.* 57 (8) (2018) 4613–4619.
- [9] S.S.-Y. Chui, S.M.-F. Lo, J.P. Charmant, A.G. Orpen, I.D. Williams, *Science* 283 (5405) (1999) 1148–1150.
- [10] L. Oar-Arteta, T. Wezendonk, X. Sun, F. Kapteijn, J. Gascon, *Mater. Chem. Front.* (2017).
- [11] Z. Bacsik, R. Atluri, A.E. Garcia-Bennett, N. Hedin, *Langmuir* 26 (12) (2010) 10013–10024.
- [12] Z. Ni, R.I. Masel, *J. Am. Chem. Soc.* 128 (38) (2006) 12394–12395.
- [13] S.H. Jung, J.H. Lee, J.W. Yoon, C. Serre, G. Férey, J.S. Chang, *Adv. Mater.* 19 (1) (2007) 121–124.
- [14] Z.-Q. Li, L.-G. Qiu, T. Xu, Y. Wu, W. Wang, Z.-Y. Wu, X. Jiang, *Mater. Lett.* 63 (1) (2009) 78–80.
- [15] M. Klimakow, P. Klobes, A.F. Thünemann, K. Rademann, F. Emmerling, *Chem. Mater.* 22 (18) (2010) 5216–5221.
- [16] K. Schlichte, T. Kratzke, S. Kaskel, *Microporous Mesoporous Mater.* 73 (1) (2004) 81–88.
- [17] L. D'Arras, C. Sassoie, L. Rozes, C. Sanchez, J. Marrot, S. Marre, C. Aymonier, *New J. Chem.* 38 (4) (2014) 1477–1483.
- [18] Z.-G. Gu, H. Fu, T. Neumann, Z.-X. Xu, W.-Q. Fu, W. Wenzel, L. Zhang, J. Zhang, C. Wöll, *ACS Nano* 10 (1) (2015) 977–983.
- [19] K.-S. Lin, A.K. Adhikari, C.-N. Ku, C.-L. Chiang, H. Kuo, *Int. J. Hydrog. Energy* 37 (18) (2012) 13865–13871.
- [20] W.W. Lestari, M. Adreane, C. Purnawan, H. Fansuri, N. Widiastuti, S.B. Rahardjo, IOP Conference Series: Materials Science and Engineering; IOP Publishing, 2016, p. 012030.
- [21] A.S. Münch, F.O. Mertens, *J. Mater. Chem.* 22 (20) (2012) 10228–10234.
- [22] I. Majchrzak-Kuceba, D. Bukalak-Gaik, *J. Therm. Anal. Calorim.* 125 (3) (2016) 1461–1466.
- [23] C. McKinstry, E.J. Cussen, A.J. Fletcher, S.V. Patwardhan, J. Sefcik, *Chem. Eng. J.* (2017).
- [24] S. Khoshhal, A.A. Ghoreysi, M. Jahanshahi, M. Mohammadi, *RSC Adv.* 5 (31) (2015) 24758–24768.
- [25] K.-Y.A. Lin, Y.-T. Hsieh, *J. Taiwan Inst. Chem. Eng.* 50 (2015) 223–228.
- [26] N. Al-Janabi, P. Hill, L. Torrente-Murciano, A. Garforth, P. Gorgojo, F. Siperstein, X. Fan, *Chem. Eng. J.* 281 (2015) 669–677.
- [27] D. Bazer-Bachi, L. Assié, V. Lecocq, B. Harbuzaru, V. Falk, *Powder Technol.* 255 (2014) 52–59.
- [28] S. Zhang, H. Liu, P. Liu, Z. Yang, X. Feng, F. Huo, X. Lu, *Nanoscale* 7 (21) (2015) 9411–9415.
- [29] S. Shen, W. Wu, K. Guo, J. Chen, *J. Mater. Sci. Technol.* 14 (4) (2007) 369–372.
- [30] X. Mu, Y. Chen, E. Lester, T. Wu, *Microporous Mesoporous Mater.* (2018).
- [31] W. Liu, Y. Xu, W. Zhou, X. Zhang, X. Cheng, H. Zhao, S. Gao, L. Huo, *J. Mater. Sci. Technol.* 33 (1) (2017) 39–46.
- [32] L. Cheng, Y. Jiang, S.-C. Qi, W. Liu, S.-F. Shan, P. Tan, X.-Q. Liu, L.-B. Sun, *Chem. Mater.* 30 (10) (2018) 3429–3437.
- [33] S. Gadipelli, Z. Guo, *Chem. Mater.* 26 (22) (2014) 6333–6338.
- [34] Y. Cheng, A. Kondo, H. Noguchi, H. Kajiro, K. Urita, T. Ohba, K. Kaneko, H. Kanoh, *Langmuir* 25 (8) (2009) 4510–4513.
- [35] A. Kathuria, M.G. Abiad, R. Auras, *Polym. Int.* 62 (8) (2013) 1144–1151.
- [36] T. Toyao, K. Liang, K. Okada, R. Ricco, M.J. Styles, Y. Tokudome, Y. Horiuchi, A.J. Hill, M. Takahashi, M. Matsuoka, *Inorg. Chem. Front.* 2 (5) (2015) 434–441.
- [37] C. Zheng, H. Ren, Z. Cui, F. Chen, G. Hong, *J. Alloy. Compd.* 477 (1) (2009) 333–336.
- [38] Y. Guo, Y. Mao, P. Hu, Y. Ying, X. Peng, *ChemistrySelect* 1 (1) (2016) 108–113.
- [39] K. Sumida, D.L. Rogow, J.A. Mason, T.M. McDonald, E.D. Bloch, Z.R. Herm, T.-H. Bae, J.R. Long, *Chem. Rev.* 112 (2) (2012) 724–781.
- [40] K. Tan, N. Nijem, Y. Gao, S. Zuluaga, J. Li, T. Thonhauser, Y.J. Chabal, *CrystEngComm* 17 (2) (2015) 247–260.
- [41] S. Ye, X. Jiang, L.-W. Ruan, B. Liu, Y.-M. Wang, J.-F. Zhu, L.-G. Qiu, *Microporous Mesoporous Mater.* 179 (2013) 191–197.
- [42] Y.-R. Lee, J. Kim, W.-S. Ahn, *Korean J. Chem. Eng.* 30 (9) (2013) 1667–1680.
- [43] M. Klimakow, P. Klobes, K. Rademann, F. Emmerling, *Microporous Mesoporous Mater.* 154 (2012) 113–118.
- [44] A. Omri, S.D. Lambert, J. Geens, F. Bennour, M. Benzina, *J. Mater. Sci. Technol.* 30 (9) (2014) 894–902.
- [45] I. Spanopoulos, I. Bratsos, C. Tampaxis, D. Vourloumis, E. Klontzas, G. Froudakis, G. Charalambopoulou, T. Steriotis, P. Trikalitis, *Chem. Commun.* 52 (69) (2016) 10559–10562.
- [46] R. Sabouni, H. Kazemian, S. Rohani, *Environ. Sci. Pollut. Res.* 21 (8) (2014) 5427–5449.
- [47] R. Chugh, P. Bajpai, H.G. Bhunia, *Carbon Dioxide Adsorpt. Metal. Org. Framew. Basolite C300* (2015).
- [48] J. Liu, Y. Wang, A.I. Benin, P. Jakubczak, R.R. Willis, M.D. LeVan, *Langmuir* 26 (17) (2010) 14301–14307.
- [49] M. Du, L. Li, M. Li, R. Si, *RSC Adv.* 6 (67) (2016) 62705–62716.
- [50] Q.M. Wang, D. Shen, M. Bülow, M.L. Lau, S. Deng, F.R. Fitch, N.O. Lemcoff, *J. Semicond. Microporous Mesoporous Mater.* 55 (2) (2002) 217–230.
- [51] M.-W. Yang, N.-C. Chen, C.-H. Huang, Y.-T. Shen, H.-S. Yang, C.-T. Chou, *Energy Procedia* 63 (2014) 2351–2358.
- [52] J. McEwen, J.-D. Hayman, A.O. Yazaydin, *Chem. Phys.* 412 (2013) 72–76.
- [53] C. Chen, Y.-R. Lee, W.-S. Ahn, *J. Nanosci. Nanotechnol.* 16 (5) (2016) 4291–4301.
- [54] S. Mane, Z.-Y. Gao, Y.-X. Li, D.-M. Xue, X.-Q. Liu, L.-B. Sun, *J. Mater. Chem. A* 5 (44) (2017) 23310–23318.
- [55] S. Nandi, P. De Luna, T.D. Daff, J. Rother, M. Liu, W. Buchanan, A.I. Hawari, T.K. Woo, R. Vaidhyanathan, *Sci. Adv.* 1 (11) (2015) e1500421.
- [56] M. Mohamedali, D. Nath, H. Ibrahim, A. Henni, Review of recent developments in CO₂ capture using solid materials: metal organic frameworks (MOFs), *Greenhouse Gases, InTech*, 2016.